Exciton-exciton annihilation in single-walled carbon nanotubes

Leonas Valkunas
Department of Chemistry, University of California, Berkeley, Berkeley, California 94720-1460, USA;
Physical Biosciences Division, Lawrence Berkeley National Laboratory, Berkeley, California 94720-1460, USA;
Institute of Physics, Savanoriu Ave. 231, 02300 Vilnius, Lithuania;
and Theoretical Physics Department, Faculty of Physics of Vilnius University, Sauletekio Ave. 9, building 3, 10222 Vilnius, Lithuania

Ying-Zhong Ma and Graham R. Fleming*
Department of Chemistry, University of California, Berkeley, Berkeley, California 94720-1460, USA
and Physical Biosciences Division, Lawrence Berkeley National Laboratory, Berkeley, California 94720-1460, USA
(Received 20 December 2005; revised manuscript received 24 February 2006; published 30 March 2006)

The femtosecond fluorescence and transient absorption kinetics recorded on selected semiconducting single-walled carbon nanotubes exhibit pronounced excitation-intensity-dependent decays as the result of exciton-exciton annihilation. A satisfactory description of the decays obtained at various excitation intensities, however, requires a time-independent annihilation rate that is valid only for extended systems with dimensionality greater than 2 in conjunction with diffusive migration of excitons. We resolved this apparent contradiction by developing a stochastic model, in which we assumed that the exciton states in semiconducting nanotubes are coherent, and the multiexciton manifolds are resonantly coupled with other excited states, which decay by subsequent linear relaxation due to electron-phonon coupling. The formalism derived from this model enables a qualitative description of the experimental results for the (9,5), (8,3), and (6,5) semiconducting single-walled carbon nanotubes.

DOI: 10.1103/PhysRevB.73.115432 PACS number(s): 78.47.+p, 71.35.−y

I. INTRODUCTION

Single-walled carbon nanotubes (SWNT) are elongated forms of the fullerene family, with small diameter and large aspect ratio. This quasi-one-dimensional (quasi-1D) substance possesses unique electronic properties, namely, quantization of the electronic structure coupled with diameter-tunable transition energy, and chirality-dependent metallic or semiconducting characteristics.[1,2] These unique electronic properties, in conjunction with the remarkable mechanical and thermal characteristics, indicate great potential for novel applications,[3] ranging from nanometer-scale conducting wires to SWNT based (opto-) electronic elements and devices. Currently, there is considerable interest in understanding the optical spectra, ultrafast dynamics, and related physical mechanisms due to their fundamental importance and direct relevance to many of the potential applications.

The physical nature of the elementary excitations in a semiconductor material differs fundamentally depending on the exciton binding energy,[4] a quantity measuring the magnitude of the Coulombic interaction between an electron and its corresponding hole. When the exciton binding energy is comparable to or smaller than the thermal energy (k_bT), the electron and hole behave as independent, uncorrelated charged carriers. In the opposite case when the exciton binding energy is larger than k_bT, the Coulombically bound electron and hole form a stable neutral exciton. In accord with these two possibilities for the nature of the elementary excitations, two theoretical approaches have been used to describe optical spectroscopic observations of semiconducting nanotubes. The first approach, which originates from the calculations of electronic structure based on a conventional one-electron approximation, attributes the optical spectra to the transitions between the van Hove singularities of the valence and conduction bands of a (quasi-) 1D system.[1,2,5–7] The resulting charged carriers, the electrons and holes, are treated as independent, uncorrelated quasiparticles. The alternative approach explicitly takes multiparticle correlation effects into account, including the Coulombic coupling between the electron and hole, resulting in an excitonic origin of the spectral features.[8,9]

Experimental studies of the excitation dynamics using ultrafast pump-probe measurements at various wavelengths[5,7,10–16] and time-resolved fluorescence measurements with sub-100 femtosecond time resolution[17–19] have recently been reported. The results were interpreted by assuming that either charged carriers[7,10] or neutral excitons are responsible for the optical spectra and ultrafast relaxation of excitations[11,13,17] In addition, the experimental results reported by different laboratories vary considerably both quantitatively and qualitatively. Several basic issues, including the "characteristic" excited-state lifetimes and their associated dynamical processes, the physical mechanism(s) governing the ultrafast relaxation, the assignments of specific spectral features identified in transient absorption spectroscopy, and the dependences of the kinetics on excitation intensity and excitation/detection wavelength, etc., are currently the focus of debate.

In a systematic study aimed at understanding the ultrafast dynamics associated with structurally distinct nanotube species, we have recently demonstrated that a model involving ultrafast exciton-exciton annihilation provides a satisfactory description of the excitation-intensity-dependent fluorescence decays recorded with sub-100 fs time resolution for several selected semiconducting nanotube species.[17] We also

showed that optically selective detection of structurally distinct tube species from a mixture of various types is possible in transient absorption spectroscopic experiments.[20] Application of femtosecond frequency-resolved transient absorption spectroscopy to a selected nanotube type, the (8,3) tube, further enabled us to reveal the spectroscopic and dynamic signatures of the annihilation.[13] Our observations provide strong experimental evidence for the excitonic nature of the elementary excitation in individual semiconducting nanotubes. Further studies allowed us to determine the exciton binding energy of the (8,3) tube to be 0.41 eV (Ref. 21) in good agreement with two photon spectroscopic studies.[22,23]

The nonlinear process of exciton-exciton annihilation profoundly influences the excitation dynamics in condensed phases at high excitation intensities.[24–27] The annihilation process is conceptually similar to a chemical reaction,[28] written as $A+A \rightarrow A$ in the case of singlet-singlet annihilation, or as $A+B \rightarrow B$ for singlet-triplet annihilation. From this similarity, it is obvious that the diffusion of the exciton can be a limiting factor for annihilation if the size of the system under consideration is extended. The corresponding dynamics is then determined by the time that two excitations need to find each other in the system. On the other hand, the rate of pair-wise reaction (static interaction) itself might be the dominant process if the actual size of the system is small in comparison with the diffusion radius of excitons (or reactants).

Theoretical approaches are well developed for two limiting cases of the ratio between the excitation diffusion radius and the actual size of the system. For extended systems, with a size which is comparable to the diffusion radius, the annihilation is sensitive to the rate of the excitation migration. In this case, multiparticle distribution functions can be used to characterize the relative distribution of excitations within an ensemble of such systems.[28,29] The natural limiting case of an infinitely large system (the approach widely used for molecular crystals) is straightforward from this description. In the opposite case, for systems with sizes much smaller than the excitation diffusion radius, the nonlinear annihilation process is no longer limited by diffusion. The excitations in such small systems equilibrate very rapidly, and the annihilation process itself is determined by the rate of annihilation between two already equilibrated excitations. The main statistical effect then is due to the distribution of the excitations in the ensemble of such systems.[26,30,31] It is noteworthy that the theory of the chemical reactions was mainly developed for the infinitely large systems,[28,29,32,33] while the size-restriction effect has been described only recently.[34] Both theoretical approaches have been well developed by and widely applied to exciton-exciton annihilation in various photosynthetic pigment-protein complexes.[26,27,30,31,35–38]

Diffusion-limited exciton-exciton annihilation is sensitive to the dimensionality of the system, resulting in a time dependence of the annihilation rate for low dimensional (less than 2) cases.[26,27,39,40] From the structural point of view, a SWNT is a (quasi-) 1D system. The large Bohr radius of excitons in comparison to the tube diameter, rules out any motion with dimensionality >1 such as along the circumference of the tube. Thus, SWNTs should be considered as strict 1D systems in terms of exciton migration. If exciton-exciton annihilation in SWNTs is governed by diffusive migration of excitons, then one would expect a time-dependent annihilation rate. This is, however, in contrast to the conclusions reached from analysis of the excitation-intensity-dependent kinetics, which clearly show a time-independent annihilation rate in semiconducting SWNT.[13,17] The time independent annihilation rate deduced from our experiments thus provides a strong indication that the process is not diffusion limited and, therefore, that coherent exciton states should be considered as the elementary excitations, which are involved in the annihilation. A theory for annihilation of coherent excitons was formulated very recently for molecular complexes consisting of many chromophores[41] and was applied to the analysis of the excitation kinetics in photosynthetic pigment-protein complexes.[42] Since this approach deals with molecular (Frenkel) excitons in systems with well-defined spectral inhomogeneity, it is not directly applicable to 1D semiconducting systems, where intramolecular relaxation channels are absent. The stochastic model suggested recently to describe carrier dynamics and nonlinear annihilation provides an important step towards a theoretical understanding of fast excitation kinetics in SWNT.[43] While this model is formally applicable to exciton-exciton annihilation, it does not describe the origin of the relaxation channels. Here a theoretical scheme appropriate for SWNT with explicit consideration of coherent exciton states will be developed and related to the experimental data obtained for several specific semiconducting nanotubes. A key feature of our description is its ability to explain the time independence of the annihilation rate.

The paper is organized as follows. Following a brief description of the experimental methods in the next section, we present the experimental results in Sec. III providing the main characteristics of exciton-exciton annihilation in semiconducting SWNT. Section IV contains the theoretical model. In Sec. V, numerical calculations are presented followed by concluding remarks in Sec. VI.

II. MATERIALS AND METHODS

A. Femtosecond fluorescence upconversion

Fluorescence upconversion experiments were performed using the setup described previously.[17,20] Briefly, the light source was a commercial regenerative Ti:sapphire amplifier with a repetition rate of 250 kHz, generating $\sim$50 fs [full width at half maximum (FWHM)] pulses centered at 800 nm. The major portion (70%) of the amplifier output was used to pump an optical parametric amplifier (OPA) to produce pulses centered at 567 and 660 nm, respectively. A dual prism compressor consisting of two SF10 prisms was employed to compensate for group velocity dispersion, producing a nearly transform-limited pulse of $\sim$30 fs FWHM. The excitation beam was then focused to a spot size of $\sim$30 μm using a lens with $f=5$ cm. The minor part of the amplifier output (30%) served as a gate pulse and was temporally delayed using a stepping-motor driven optical delay stage. A sample cell of 1.0 mm pathlength was placed at one focus of an ellipsoidal reflector, which collected the spontaneous emission from the sample and focused it into an upconversion crystal (0.5 mm BBO) positioned at the other fo-

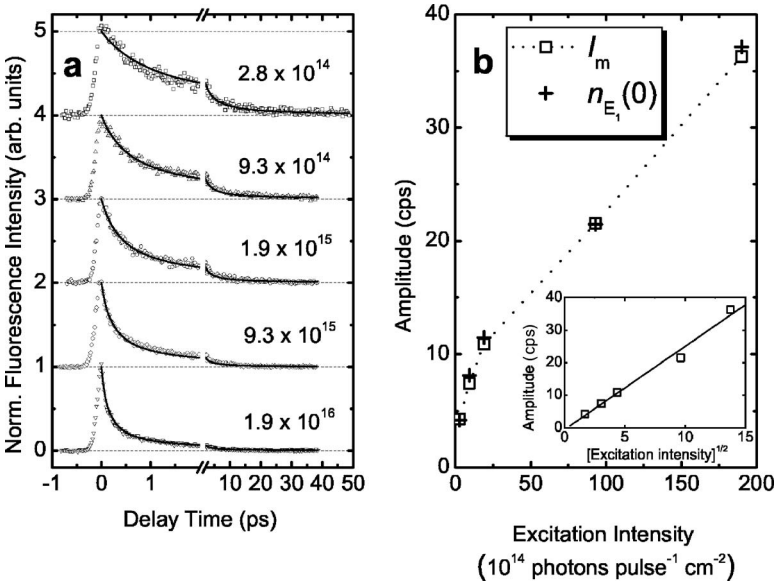

FIG. 1. (a) Normalized time-resolved fluorescence intensity for the (9,5) tube structure at different excitation intensities (in photons $\text{pulse}^{-1}\ \text{cm}^{-2}$). The solid lines represent global fits according to the solution of Eq. (1). (b) Plot of the maximum fluorescence intensity I_m and the fitted parameter $n_{E_1}(0)$ vs the excitation intensities. The dotted line is drawn to guide the eye. The inset shows I_m plotted vs the square root of the excitation intensity, and the solid line represents a linear fit.

cus. The residual pump beam, after passing through the sample cell, was blocked with a small metal rod at a point between the reflector and crystal allowing the majority of the collected fluorescence to pass. The upconverted fluorescence was collected with a lens and focused, after spatial filtering, into the entrance slit of a double grating monochromator. Finally, the upconverted light was detected with a photomultiplier tube connected with a gated photon counter (Stanford Research Systems SR400). The polarization of the excitation beam was set at the magic angle (54.7 deg) with respect to the gate beam using an achromatic $\lambda/2$ plate. The instrument response function (IRF) was recorded by upconverting the instantaneous water Raman scattering of the excitation light. The FWHM of the IRF was 98 and 120 fs for excitation at 567 and 660 nm, respectively.

B. Femtosecond frequency-resolved transient absorption

The same laser system was used in the frequency-resolved transient absorption experiments. The visible and near-infrared (NIR) pump pulses were from the signal and idler outputs of the OPA, respectively. The pump beam was focused to a spot size of $\sim 300\ \mu$m at the sample position. To monitor the pump-induced change of absorbance, we employed a single-filament white light continuum generated in a sapphire plate of 2 mm thickness using the minor portion of the amplifier output. The remaining fundamental in the continuum was spectrally filtered using either a short-wave length or a long-wavelength cutoff filter (CVI, SP750/LP850). The continuum was then split into two separate beams, a probe and a reference, which were focused to a spot of $\sim 200\ \mu$m with two spherical mirrors with $f=20$ cm. The probe and reference beams were vertically displaced on the sample cell by ~ 4 mm and only the probe beam was spatially overlapped with the pump beam. After passing through the sample, the probe and reference were focused onto the entrance slits of a spectrograph (SpectroPro 300i) and detected with a Peltier cooled charge coupled device (CCD) at series of time delays between the pump and probe pulses. The raw data collected at each time delay were binned to a spectral resolution of 2.15 nm to enhance signal-to-noise, and correction was also made for the group velocity dispersion of the probing continuum. Alternatively, frequency-integrated kinetics at selected probe wavelengths were recorded with a detection bandwidth of 4 nm by a silicon photodiode and a lock-in amplifier. The polarization of the pump beam was set to the magic angle (54.7 deg) with respect to the probe beam. A typical cross correlation between pump and probe pulses had a temporal width of about 100 fs.

C. Sample preparation

The SWNT material was produced by a HiPco-type generator, and the same procedure as described previously was used to prepare a sample rich in individual nanotubes in a surfactant-water system (SDS in H_2O).[44] The typical sample optical density (OD) was about 0.15 per mm. During data acquisition, the samples were circulated slowly using a peristaltic pump in the fluorescence experiment, while in the transient absorption experiment a sample cell with 1 mm pathlength was continuously translated vertically. Stability of the sample was checked by recording the absorption spectra before and after the time-resolved measurements, showing no observable change.

III. EXPERIMENTAL RESULTS

Figure 1(a) shows the fluorescence kinetics detected at 1244 nm upon excitation at 660 nm for five different excitation densities. These excitation and emission wavelengths are resonant with the second (E_2) and the first (E_1) electronic transitions of (9,5) tube type, and thus allowing spectral selection of this single tube type from a mixture of many tube types in the sample, including both metallic and semiconducting nanotubes. The fluorescence decays show strong intensity dependence, with faster decays as excitation intensity increases. At the highest excitation intensity, the majority of excited population disappears within the first 500 fs as seen

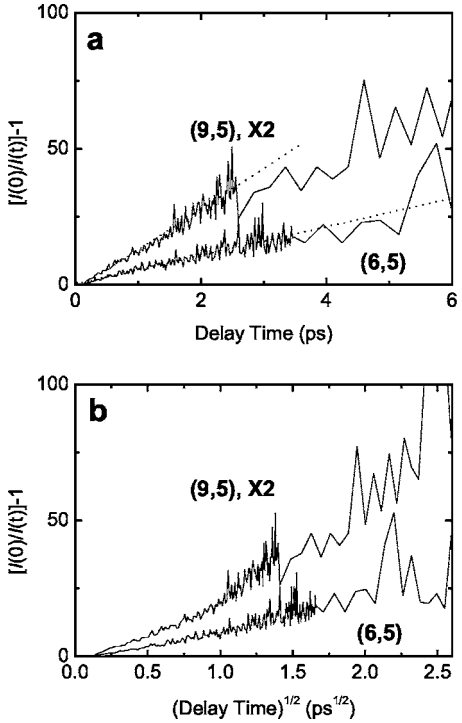

FIG. 2. (a) Plot of the inverse of the normalized intensity vs delay time for the data measured for (9,5) and (6,5) tubes under the highest excitation intensity. (b) The same data as in (a) plotted as the inverse of normalized intensity vs the square root of delay time.

from the corresponding kinetics [Fig. 1(a)]. In addition, a nonlinear dependence of the maximum amplitude of the fluorescence signal on the excitation intensity is observed [Fig. 1(b)]. We found that the maximum amplitude scales linearly with the square root of excitation intensity [see inset in Fig. 1(b)]. Similar decay behavior was observed for all other selected tube species, i.e., (8,3), (6,5), (7,5), and (7,6) (data not shown), which emit at 950, 975, 1024, and 1119 nm, respectively.

This strong excitation intensity dependence of the fluorescence decay in conjunction with the nonlinear correlation between the maximum fluorescence amplitude and the excitation intensity are indicative of occurrence of exciton-exciton annihilation. As demonstrated previously,[17] the fluorescence decays obtained at different excitation intensities can be satisfactorily described by a simple rate equation

$$\frac{dn_{ex}(t)}{dt} = -\frac{1}{2}\gamma n_{ex}^2(t), \tag{1}$$

where $n_{ex}(t)$ is the population of excitons and γ is the rate constant for exciton-exciton annihilation. Equation (1) represents a special case of exciton-exciton annihilation in an extended system, with predominant nonlinear relaxation.[26,27] Since the fluorescence intensity is proportional to the population of excitons, the solution of Eq. (1), $[n_{ex}(0)/n_{ex}(t)]-1 = \gamma n_{ex}(0)t$ [here $n_{ex}(0)$ is the initial population of excitons], predicts a linear relation between the inverse of the normalized fluorescence decay and the delay time, t. This linear dependence is indeed observed. As an example, Fig. 2(a) shows the experimental data obtained for the (6,5) and (9,5) tube types under the highest pump intensity.

In addition to describing the fluorescence decays, we further found that Eq. (1) can also describe the transient absorption kinetics measured for selected tube species. Figure 3(a) shows the kinetics probed for the (8,3) tube under three different pump intensities. These data are collected by resonantly exciting the (8,3) E_2 transition at 660 nm and by tuning the probe wavelength to the (8,3) E_1 transition at 953 nm. The kinetic decays show a similar dependence on pump intensity as the fluorescence [Fig. 1(a)], i.e., a faster decay with increasing pump intensity. The data recorded at the highest pump intensity are plotted in Fig. 3(b) as the inverse of the signal amplitude, $[\Delta OD_0/\Delta OD(t)]$, versus delay time t, giving again a good linear dependence except at short decay times (<1 ps). Note that ΔOD_0 and $\Delta OD(t)$ are the maximum transient absorbance signal and the transient absorption at t, respectively. While the ΔOD_0 differs from the $\Delta OD(0)$, both are constants and therefore use of either quantity will not alter the time dependence of the signals. A linear dependence is also found for the kinetics measured by directly pumping the E_1 transition of (8,3) tube [Fig. 3(c)] as shown in Fig. 3(d), where the data are plotted as the inverse of the transient absorption amplitude versus the delay time.

While Eq. (1) provides a description for the excitation-intensity-dependent fluorescence and transient absorption decays, an essential prerequisite for the application of this equation is not satisfied. Equation (1) or its generalized form, with one or more linear terms in the right-hand side, is applicable to exciton-exciton annihilation in an extended system whose size is comparable with or larger than the exciton diffusion radius.[26,27] For such systems, it is generally assumed that exciton-exciton annihilation is diffusion limited, and the corresponding annihilation rate depends on the dimensionality of the system. Use of a time-independent annihilation rate is appropriate only for a system with a dimensionality (d) that is equal to or greater than 2. For systems with reduced dimension such as SWNT, the annihilation rate becomes time dependent, given by $\gamma = \gamma_0/t^{1-d/2}$. Accordingly, Eq. (1) should be rewritten for a 1D SWNT as follows:

$$\frac{dn_{ex}(t)}{dt} = -\frac{1}{2}\gamma_0 t^{-1/2} n_{ex}^2(t). \tag{2}$$

As the fluorescence intensity is proportional to the population of excitons, the solution of Eq. (2), $[n_{ex}(0)/n_{ex}(t)]-1 = n_{ex}(0)\gamma_0\sqrt{t}$, suggests a linear dependence of the inverse of the normalized fluorescence kinetics on $\sqrt{t}$. The predicted linear dependence is not in accord with the experimental data as shown in Fig. 2(b), plotted as the inverse of intensity over the square root of delay time, $\sqrt{t}$. In addition, clear deviations from linearity are also observed for the transient absorption data shown in Figs. 3(a) and 3(c), plotted as $[\Delta OD_0/\Delta OD(t)]^2$ vs t [see Figs. 3(b) and 3(d), open circles]. The significant deviation from linearity leads to a contradiction: the fluorescence kinetics recorded at high excitation conditions can be satisfactorily described by an exciton-exciton annihilation formula with a time-independent annihilation rate, which is valid strictly for an extended system

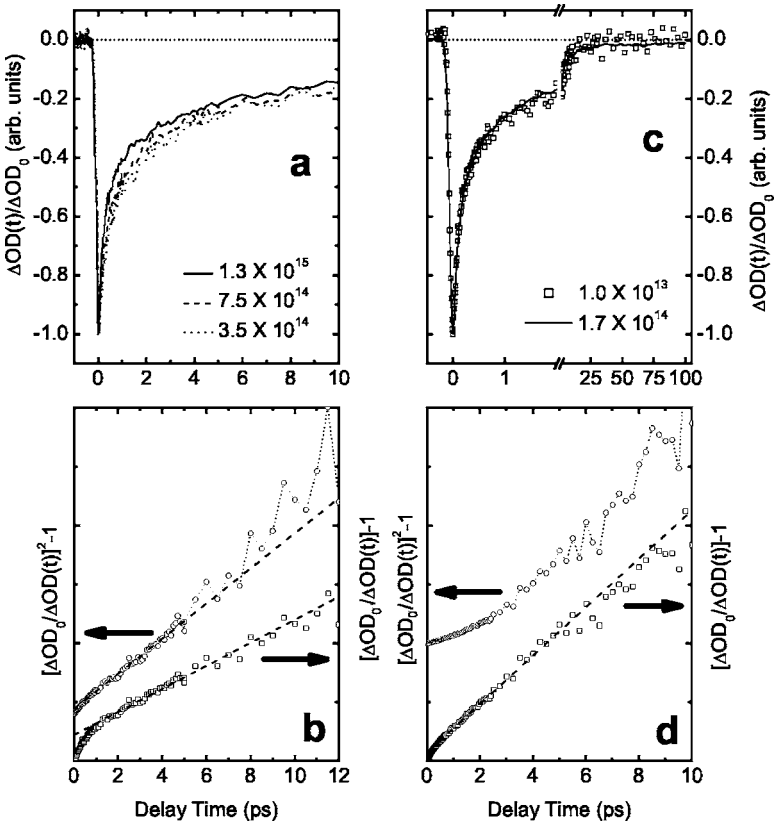

FIG. 3. (a) Transient absorption kinetics probed at 953 nm at three different pump pulse intensities at 660 nm (in photons $\text{pulse}^{-1}\,\text{cm}^{-2}$). (b) Plot of $\{[\Delta\text{OD}_0/\Delta\text{OD}(t)]-1\}$ (squares), and $\{[\Delta\text{OD}_0/\Delta\text{OD}(t)]^2-1\}$ (circles) vs delay time for the data recorded at the highest pump intensity as shown in (a). (c) Transient absorption kinetics probed at 953 nm at two different intensities of the pump pulses at 953 nm (in photons $\text{pulse}^{-1}\,\text{cm}^{-2}$). (d) Plot of $\{[\Delta\text{OD}_0/\Delta\text{OD}(t)]-1\}$ (squares), and $\{[\Delta\text{OD}_0/\Delta\text{OD}(t)]^2-1\}$ (circles) vs delay time for the data recorded at the higher pump intensity as shown in (c). For ease of comparison, all the kinetics shown in (a) and (c) are normalized at the signal maxima. The dashed lines in (b) and (d) represent linear fits of the data.

with a dimensionality equal to or greater than 2 only. However the exciton Bohr radius is larger than the tube diameter,[8,9] ruling out any motion of excitons transverse to the tube axis. The flaw in the analysis must stem from the assumption of diffusive migration of the excitons.

Before exploring the reason causing this flaw, it is important to keep in mind that exciton-exciton annihilation in semiconducting SWNT has several unique features.[13] (1) Electronically resonant excitation of the E_1 state of the (8,3) tube at 953 nm induces an instantaneous spectral response at 660 nm, the location of the corresponding E_2 transition. The assignment of this response to the E_2 transition is confirmed by the similarity between the kinetics probed at 660 nm for excitation of the E_1 state and by direct E_2 excitation (data not shown). (2) The dependence of the amplitude of the transient absorption signal on the intensity of pump pulses at 953 nm differs for the kinetics probed at 660 and 953 nm. The former exhibits a linear dependence, whereas a saturating behavior is seen for the data obtained with a 953 nm probe pulse [Fig. 4(a)]. (3) The kinetics probed at 660 and 953 nm upon resonant excitation of the E_1 transition [Fig. 4(b)] are strongly correlated with each other. This correlation is manifested by an excellent match between the squared profile of the kinetics recorded at 953 nm and the kinetics measured at 660 nm [Fig. 4(c)]. All these remarkable features can be understood by considering the annihilation of two E_1 excitons, which results in disappearance of both excitons with the simultaneous induction of population into higher excited states located in the vicinity of the doubly E_1 exciton state. The subsequent rapid relaxation leads to population of the E_2 state, and in turn its concomitant spectral response. We refer to our previous work for a detailed theoretical description and qualitative interpretation.[13]

The time scales associated with exciton-exciton annihilation in semiconducting nanotubes are another notable feature of the nonlinear relaxation. As shown in Fig. 5, the annihilation process occurs extremely rapidly, manifested by the saturating behavior of the maximum amplitude of the transient absorption signal with increasing pump intensity as the result of rapid annihilation within the pulse duration, and additionally by very rapid initial decay of the kinetics. For instance, at a delay time of 300 fs, approximately half and one-third of the exciton population has already decayed for (8,3) and (6,5) tubes, respectively. This ultrafast exciton-exciton annihilation is strikingly distinct from other nanoscale systems such as quantum wires and rods, whose optical spectra and excitation dynamics are also determined by excitons.[45] The annihilation in these materials occurs on a time scale that is at least one order of magnitude longer than in SWNT.[45]

IV. THEORETICAL MODELING

As it is clear from the experimental data presented above, a diffusion limited exciton-exciton annihilation description is not applicable for (quasi-)1D semiconducting nanotubes since (i) the annihilation rate is time-independent and (ii) the annihilation rate is extremely fast. Instead we consider coherent exciton annihilation, where the coherence length of the optically generated excitons is of a similar size to that of the nanotube. In this case the exciton band of an extended SWNT (of submicron length) can be treated as a supermol-

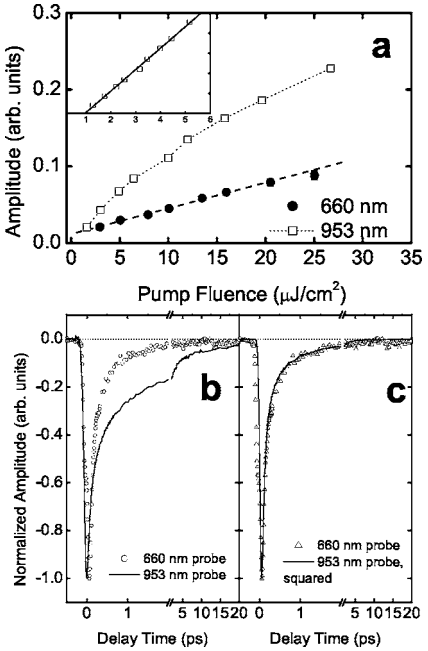

FIG. 4. (a) Plot of the maximum amplitude of the transient absorption kinetics probed at 660 nm (filled circles) and 953 nm (open squares) vs the intensity of the pump pulses at 953 nm. The dashed line is the linear fit of the data obtained with a 660 nm probe, and the dotted line is drawn to guide the eye for the data obtained with a 953 nm probe. The inset shows the 953 nm data, plotted vs the scale of square root of pump intensity. The solid line represents the linear fit. (b) Kinetics probed at 660 (open circles) and 953 nm upon resonant excitation of the E_1 transition of the (8,3) tube at 953 nm. (c) Comparison of the squared profile at 953 nm (solid line) and the kinetics at 660 nm, both data are recorded with the 953 nm excitation. All kinetics shown in (b) and (c) are normalized at the signal maxima.

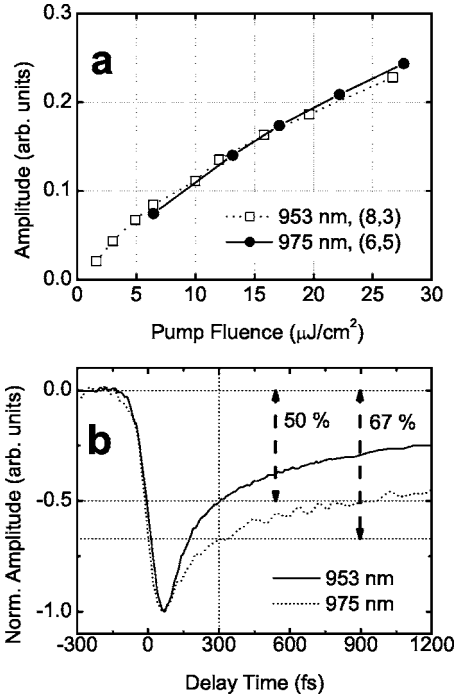

FIG. 5. (a) Plot of the maximum amplitude of the transient absorption kinetics probed at 975 nm (filled circles) and 953 nm (open squares) vs the intensity of the pump pulses centered at 953 nm. The solid and dotted lines are drawn to guide the eye. (b) The early time behavior of transient absorption kinetics probed at 975 nm (dashed line) and 953 nm (solid line), both curves were recorded with pulse pulses centered at 953 nm. The kinetics are normalized at the signal maxima. The dotted lines are drawn to highlight the initial rapid decay of the signal amplitudes at 300 fs.

ecule containing many states, which can be populated by optical excitation with an intense pulse. Since the size of the SWNT is comparable to the excitation wavelength, the excitation evolution is then determined by the molecular orbitals responsible for the collective exciton states and by energy relaxation due to the exciton-phonon interaction. As the result of the multiexciton population, an additional channel responsible for very fast relaxation due to exciton-exciton annihilation opens up.

In order to describe this type of exciton-exciton annihilation, other excited states, which are coupled with the multiexciton manifolds, should be taken into account in addition to the multiexciton manifolds characteristic of the system under consideration. The electronic structure of a semiconducting tube is usually considered to be composed of few excitonic bands, and mostly only the E_1 and E_2 are needed to interpret experimental data [see Fig. 6(a)]. However, detailed calculations of the electronic structure using various methods have shown the presence of a large number of extra excitonic states for each of the commonly referred exciton band.[46–48] In analogy to the energy levels in a 1D hydrogen atom,[49] these states form several subgroups corresponding to a different principal quantum number ($n=0,1,2,\ldots$) and symmetry (the exciton envelope function is either even or odd with respect to $z\rightarrow -z$ where the z-direction is along the tube axis[23,50]). On the top of each exciton manifold, there is an electron-hole continuum. While most of these extra states are optically dark or carry very small oscillator strengths, their presence can have profound effects on the spectroscopic properties of nanotubes, in particular, excited-state dynamics such as exciton-exciton annihilation. It is noteworthy that the only requirement for efficient exciton-exciton annihilation is resonant coupling between the multiexciton states and additional states, allowing the annihilation to be effectively independent of the nature of the exciton states such as degeneracy and parity.

Depending on the pump pulse intensity the time evolution of the excited nanotubes consists of both *linear* relaxation and *nonlinear* relaxation.[13,17] As it was already outlined, the nonlinear relaxation results from the interaction of multiple excitons, producing exciton-exciton annihilation via resonant population of the coupled manifold of electronic excitations in the system. Therefore, we consider a stochastic model consisting of a manifold of optically accessible excitons, i, and a manifold of states, $\bar{i}$, that can be accessed via exciton-exciton annihilation [Fig. 6(b)]. The time evolution of the probability that the system contains i excitons, P_i, i.e., the system is in the ith exciton manifold, and the probability of the population of the $\bar{i}$th manifold, $\bar{P}_i$, can be defined by the Master equation approach,[51] resulting in the following set of equations:

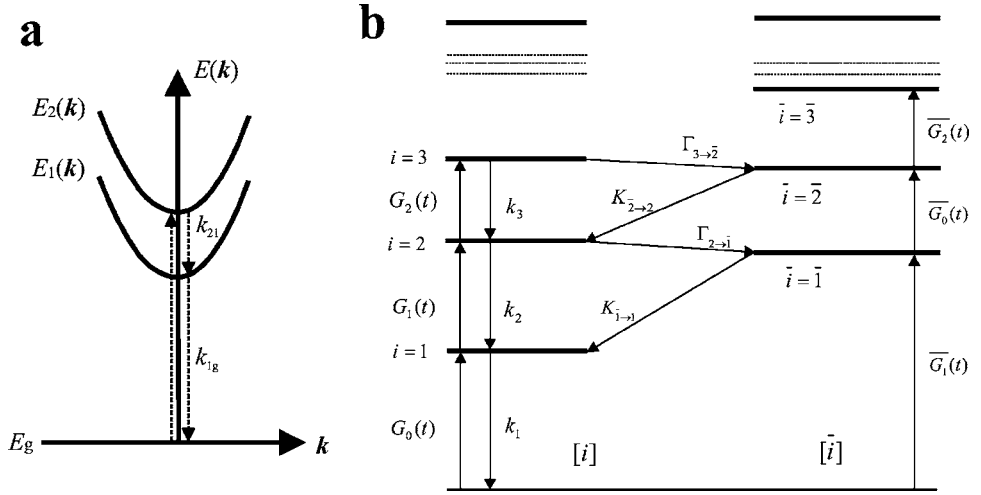

FIG. 6. (a) Schematic representation of the excitonic states in a semiconducting SWNT. E_g and $E_i(k)$ represent the ground state and the ith exciton band, respectively, k is the exciton center-of-mass momentum. The downward arrows depict the relaxation processes following an optical excitation of the $E_2(k)$ state denoted by an upward arrow. (b) Kinetic scheme for a multiexcitation manifold. i denotes the number of excitons under consideration, while $\bar{i}$ describes other excited states which are interacting with the corresponding multiexciton manifold. The transition rate between these states is given by $\Gamma_{i+1\to\bar{i}}$ and $K^{-}_{\bar{i}\to i}$ while k_i defines the relaxation within the ith exciton manifold caused by linear exciton relaxation. $G_i(t)$ and $\bar{G}_i(t)$ determine the excitation generation rate from the ith and $\bar{i}$th manifolds, respectively.

$$\frac{dP_0}{dt} = -G_0(t)P_0 - \bar{G}_0P_0 + k_1P_1, \tag{3a}$$

$$\frac{dP_1}{dt} = G_0(t)P_0 - G_1(t)P_1 - k_1P_1 + k_2P_2 + K^{-}_{\bar{1}\to 1}\bar{P}_1, \tag{3b}$$

$$\frac{dP_2}{dt} = G_1(t)P_1 - G_2(t)P_2 - (k_2 + \Gamma_{2\to\bar{1}})P_2 + k_3P_3 + K^{-}_{\bar{2}\to 2}\bar{P}_2, \tag{3c}$$

$$\frac{d\bar{P}_1}{dt} = \bar{G}_0(t)P_0 - \bar{G}_1(t)\bar{P}_1 + \Gamma_{2\to\bar{1}}P_2 - K^{-}_{\bar{1}\to 1}\bar{P}_1 \tag{3d}$$

$$\frac{d\bar{P}_2}{dt} = \bar{G}_1(t)\bar{P}_1 - \bar{G}_2(t)\bar{P}_2 + \Gamma_{3\to\bar{2}}P_3 - K^{-}_{\bar{2}\to 2}\bar{P}_2, \tag{3e}$$

etc., where $G_i(t)$ is the exciton generation rate in a system already containing i excitons, k_i is the linear exciton relaxation rate within the manifold of i excitons, $\Gamma_{i+1\to\bar{i}}$ is the transition rate between the $i+1$th exciton manifold to the $\bar{i}$th manifold of the system, $K^{-}_{\bar{i}\to i}$ determines the relaxation rate between the $\bar{i}$th manifold and the ith exciton manifold [see Fig. 6(b)]. The total exciton population (or the exciton concentration in the ensemble of the SWNT under consideration) then is determined by

$$n(t) = \sum_i iP_i(t). \tag{4}$$

Equation (3) satisfies the conservation law for the total excitation probability, i.e.,

$$\frac{d\sum_i (P_i + \bar{P}_i)}{dt} = 0. \tag{5}$$

The exciton-exciton annihilation process according to this scheme results from a two-step processes: a transition $i+1 \to \bar{i}$ with a rate defined by $\Gamma_{i+1\to\bar{i}}$ and a subsequent transition $\bar{i}\to i$ characterized by rate $K^{-}_{\bar{i}\to i}$. Since the exciton states are determined by diagonalization of the exciton Hamiltonian, neglecting coupling of exciton manifolds to other excited states defined as $\bar{i}$,[8,9] the $\Gamma_{i+1\to\bar{i}}$ value for the case of $i=1$, can be determined via the golden rule for a coupling of V,

$$\Gamma_{2\to\bar{1}} = \frac{2\pi}{\hbar}\sum_{k_1,k_2}\rho_{k_1k_2}|\langle k_1,k_2,2|V|\bar{1},k_1+k_2\rangle|^2 \times \delta[\epsilon_2(k_1,k_2) - E^{-}_{\bar{1}}(k_1+k_2)], \tag{6}$$

where $\rho_{k_1k_2}$ is the probability of population of the k_1 and k_2-exciton states in the 2-exciton manifold, which is described by the $|2,k_1,k_2\rangle$ wave function and $\epsilon_2(k_1,k_2)$ eigenenergy (here $k_{1,2}$ determines the momentum of the center-of-mass of the excitons involved in the annihilation), $|\bar{1},K\rangle$ and $E^{-}_{\bar{1}}(K)$ are the wave function and eigenenergy of the $\bar{1}$ excitation, respectively, and V is the operator determining the coupling between those states. In addition, momentum conservation resulting in $K=k_1+k_2$ is also taken into account. Transition rates for the case of $i>1$ can be similarly defined.

Relaxation rates $K^{-}_{\bar{i}\to i}$ are caused by the electron-phonon interaction producing nonadiabatic coupling of the electronic states of the system. According to the experimental observations with <100 fs time resolution the relaxation from higher excited states of SWNT occurs on a time scale of

$\leqslant$50 fs.[17,52] Evidently, if those relaxation rates are very large (in comparison with the time resolution of the processes under investigation), and in the absence of optical transitions from the $\bar{i}$th states with $\bar{i} \geqslant 1$, i.g. $\bar{G}_i(t)=0$, then the probabilities $\bar{P}_i$ are directly driven by probabilities P_{i+1} as follows from Eq. (3e)

$$\bar{P}_i = \frac{\Gamma_{i+1\to\bar{i}}}{K^{-}_{\bar{i}\to i}} P_{i+1}. \tag{7}$$

By substituting these expressions into Eq. (3a), we get

$$\frac{dP_0}{dt} = -[G_0(t) + \bar{G}_0(t)]P_0 + k_1 P_1,$$

$$\frac{dP_1}{dt} = G_0(t)P_0 - G_1(t)P_1 + \frac{\bar{G}_0}{K^{-}_{\bar{1}\to 1}} P_0 - k_1 P_1 + (k_2 + \Gamma_{2\to\bar{1}})P_2,$$

$$\frac{dP_2}{dt} = G_1(t)P_1 - G_2(t)P_2 - (k_2 + \Gamma_{2\to\bar{1}})P_2 + (k_3 + \Gamma_{3\to\bar{2}})P_3, \tag{8}$$

etc. Thus, $\Gamma_{i+1\to\bar{i}}$ are rate factors determining the relaxation channel resulted from exciton-exciton annihilation (in addition to the linear relaxation processes, defined as k_i). By assuming that the annihilation process from the multiexciton manifold is driven by the two-exciton relaxation [see Eq. (6)], the exciton distribution is defined by the statistical number of relaxation pathways, resulting in the following relationship:

$$\Gamma_{i+1\to\bar{i}} = (i+1)i\Gamma_{2\to\bar{1}} \equiv (i+1)i\Gamma. \tag{9}$$

A similar relationship can be obtained for the linear relaxation rates: $k_i = ik_1 \equiv ik$, and then Eq. (8) can be presented in the following generalized form:

$$\frac{dP_1}{dt} = G_0(t)P_0 - G_1(t)P_1 + \frac{\bar{G}_0}{K^{-}_{\bar{1}\to 1}} P_0 - kP_1 + (2k + 2\Gamma)P_2$$

and

$$\frac{dP_i}{dt} = G_{i-1}(t)P_{i-1} - G_i(t)P_i - [ik + i(i-1)\Gamma]P_i + [(i+1)k + (i+1)i\Gamma]P_{i+1} \tag{10}$$

for $i > 1$. For fast exciton-exciton relaxation/annihilation rates in extended nanotubes,[13] phase space filling is not reached, therefore we can assume that $G_i(t)$ is independent of i. Then for the population determined by Eq. (4), we will obtain the following kinetic equation:

$$\frac{dn}{dt} = G(t) + \left(\frac{\bar{G}_0}{K^{-}_{\bar{1}\to 1}}\right) P_0 - kn - \Gamma\langle i(i-1)\rangle, \tag{11}$$

where

$$\langle i(i-1)\rangle = \sum_i i(i-1)P_i \tag{12}$$

is the correlation function of the exciton population in the system. For the latter we apply the following approximation:

$$\langle i(i-1)\rangle = \langle i\rangle^2 \equiv n^2, \tag{13}$$

which strictly holds for a Poisson distribution for P_i. Accordingly, Eq. (11) leads to a kinetic equation determining the annihilation kinetics of the same form as Eq. (1),

$$\frac{dn}{dt} = G(t) + \left(\frac{\bar{G}_0}{K^{-}_{\bar{1}\to 1}}\right) P_0 - kn - \Gamma n^2, \tag{14}$$

where $\Gamma = \gamma/2$ and $n \equiv n_{ex}$ by comparing with Eq. (1). In the case of resonance excitation of an exciton state the first term in Eq. (14) determines direct exciton generation, while the second one describes two-step exciton generation via direct optical population of the $\bar{1}$th state with a subsequent fast relaxation to the one-exciton state. This can be important at high excitation intensities, when, for instance, two-photon absorption results in population of the $\bar{1}$th state.

Equation (3) can be also used to describe the exciton generation/recombination processes in other systems where the relaxation channels caused by the exciton-phonon interaction are not so fast. Indeed, in the opposite limiting case, when $\Gamma_{2\to\bar{1}}$ is much faster than the relaxation rates $K^{-}_{\bar{i}\to i}$, the population of the multiexciton manifolds is substantially depleted and all population of excitations is predominantly on the $\bar{i}$ states. Then the set of following equations is derived from the set of Eq. (3),

$$\frac{dP_0}{dt} = -G_0(t)P_0 - \bar{G}_0 P_0 + k_1 P_1,$$

$$\frac{dP_1}{dt} = G_0(t)P_0 - G_1(t)P_1 - k_1 P_1 + \bar{k}_2 \bar{P}_2 + K^{-}_{\bar{1}\to 1}\bar{P}_1,$$

$$\frac{d\bar{P}_1}{dt} = \bar{G}_0(t)P_0 - \bar{G}_1(t)\bar{P}_1 + K^{-}_{\bar{2}\to 2}\bar{P}_2,$$

$$\frac{d\bar{P}_2}{dt} = \bar{G}_1(t)\bar{P}_1 - \bar{G}_2(t)\bar{P}_2 + K^{-}_{\bar{3}\to 3}\bar{P}_3 - K^{-}_{\bar{2}\to 2}\bar{P}_2, \tag{15}$$

etc., where the following definition is introduced:

$$\bar{k}_2 = k_2 \frac{K^{-}_{\bar{2}\to 2}}{\Gamma_{2\to\bar{1}}}. \tag{16}$$

Now, in order to obtain the exciton-exciton annihilation term $\left(\propto \frac{\gamma}{2} n^2\right)$ in the kinetic equation of the exciton population, similar relationships between $K^{-}_{\bar{i}\to i}$ to those presented in Eq. 7 can be assumed, i.e., $K^{-}_{\bar{i}\to i} = i^2 K^{-}_{\bar{1}\to 1} \equiv i^2 \frac{\gamma}{2}$. Then the term determining the exciton-exciton annihilation rate in the corresponding kinetic equation for populations becomes $-\frac{\gamma}{2}\langle i^2\rangle$. By using the following approximation: $\langle i^2\rangle \approx \langle i\rangle^2 = n^2$, the conventional exciton-exciton annihilation term is obtained,

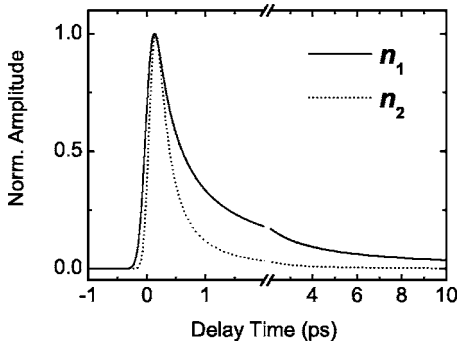

FIG. 7. The time evolution of the populations of the E_1 (solid line) and E_2 (dashed line) excitonic states calculated numerically with Eq. (20). The data are normalized at the maximum populations.

where in this case the population of excitation has to be redefined accordingly by:

$$n = \sum_i i(P_i + \bar{P}_{i-1}). \tag{17}$$

Since the $K_{\bar{i}\to i}$ relaxation rate is faster for larger i values, the intermediate situation, when $K_{\bar{1}\to 1}$ is not very large (in comparison with the time resolution of the experiment) and $K_{\bar{i}\to i}$ (for $i>1$) produces relaxations that are faster than the experimental time scale, can be also considered. In this case the kinetics of the $\bar{1}$ state population needs to be taken into account. Using the same type of approach as that giving Eq. (14) from Eq. (3), the following kinetic equations can be derived:

$$\frac{dn}{dt} = G(t) - kn - \Gamma n^2 - 2\Gamma P_2 + K\bar{P}_1,$$

$$\frac{d\bar{P}_1}{dt} = \bar{G}_0(t)P_0 - \bar{G}_1(t)\bar{P}_1 + 2\Gamma P_2 - K\bar{P}_1, \tag{18}$$

where $K=K_{\bar{1}\to 1}$, and n is the exciton population defined by Eq. (4). To obtain a closed set of equations for populations the following approximation of the two-exciton population based on definition of correlation function given by Eq. (12) can be used

$$n^2 = \langle i(i-1)\rangle \equiv \sum_i i(i-1)P_i \cong 2P_2. \tag{19}$$

Similarly introducing the definition of the $\bar{1}$ state, $\bar{n}\approx\bar{P}_1$ (since the population of other $\bar{i}$ manifolds is negligibly small in this case) from Eq. (16) we obtain the following set of equations:

$$\frac{dn}{dt} = G(t) - kn - 2\Gamma n^2 + K\bar{n},$$

$$\frac{d\bar{n}}{dt} = \bar{G}_0(t)P_0 - \bar{G}_1(t)\bar{n} + \Gamma n^2 - k\bar{n}. \tag{20}$$

According to our model, the transient spectrum, $\Delta\mathrm{OD}(\lambda,t)$, is determined by the kinetics of the populations of the excited states and the absorption spectra of the ground and excited states

$$\Delta\mathrm{OD}(\lambda,t) \propto \sum_i n_i(t)[\sigma_i^{ESA}(\lambda) - \sigma_i^{SE}(\lambda) - \sigma_0(\lambda)], \tag{21}$$

where $\sigma_0(\lambda)$ is the ground state absorption spectrum (λ is the wavelength of the probe pulse), $\sigma_i^{ESA}(\lambda)$ and $\sigma_i^{SE}(\lambda)$ are the cross sections for excited state absorption and stimulated emission of the ith excited state, respectively, $n_i(t)$ determines the time evolution of the ith excited state population (i enumerates the exciton states as well as the other type of states populated as a result of exciton-exciton annihilation). In the case where both these excited states being populated, with corresponding kinetics described by Eq. (20), from Eq. (21) we get:

$$\Delta\mathrm{OD}(\lambda,t) \propto n(t)[\sigma^{ESA}(\lambda) - \sigma^{SE}(\lambda) - \sigma_0(\lambda)] + \bar{n}(t)[\bar{\sigma}^{ESA}(\lambda) - \bar{\sigma}^{SE}(\lambda) - \sigma_0(\lambda)], \tag{22}$$

which suggests that different kinetics will be observed at different wavelengths even for the same tube type, as is observed experimentally.[13,21]

V. DISCUSSION

The formulation derived above shows that exciton-exciton annihilation involving coherent exciton states in 1D semiconducting nanotubes is characterized by a time-independent annihilation rate, and a simple rate equation analogous to the one describing the diffusion-limited annihilation in an extended system with a dimensionality greater than 2 is obtained. This result removes the apparent contradiction from our analysis of the experimental data (see Fig. 3), since exciton diffusion is not the limiting step in the nonlinear relaxation process. The resulting rate equation can now be applied to analyze the excitation-intensity-dependent exciton dynamics in semiconducting SWNT, and perhaps also in other nanoscale systems with reduced dimension such as quantum dots and rods.

So far our model has been constructed with an abstract set of states. We now connect the model to the actual electronic structure of a semiconducting SWNT. We assume in constructing the kinetic scheme shown in Fig. 6(b) that the annihilation involves excitons of the energetically lowest electronic state, the E_1 exciton state in our notation. The formulas derived are therefore directly applicable to the kinetics probed in the E_1 transition following either direct optical excitation of this transition or via a higher-lying excited state with the rapid relaxation to the E_1 state.[17,52] Moreover, we attribute all higher excited states including the E_2 exciton state, the latter enumerated as $\bar{1}$, as well as higher excited states to a separate group of states $\bar{i}$ [Fig. 6(b)]. According to our model, exciton-exciton annihilation is caused by the interaction between the multiexciton states (designated by i) and the $\bar{i}$ excited states of the system. Since the $E_2\to E_1$ relaxation as well as the relaxation within the same type of

excitons (given by $K_{\bar{i}\to i}$) is very fast (<50 fs),[17,52] the conditions required for deriving Eq. (14) are fulfilled. Comparing Eq. (14) with Eq. (1), we get $\gamma=2\Gamma$, where the Γ is defined by Eq. (6). Depending on the excitation wavelength, either the generation term $G(t)$ (in the case of resonant excitation of the E_1 state) or $\bar{G}_0$ (for resonant excitation of the E_2 state) plays a dominant role.

The coupling between the electronic states of different manifolds via exciton-exciton annihilation further results in differing intensity dependence of the corresponding populations. As follows from Eq. (20), when the excitation pulse is resonant with an excitonic transition and hence $\bar{G}_i(t)=0$, the population at the delay time corresponding to the excitation pulse maximum, t_0, is

$$\bar{n} \cong \frac{\Gamma}{K} n^2. \tag{23}$$

When the major component of relaxation is exciton-exciton annihilation, the stationary solution of the first equation of Eq. (20) results in

$$n^2 \cong \frac{1}{\Gamma} G_0(t_0). \tag{24}$$

Substituting Eq. (24) into Eq. (23), we obtain

$$\bar{n} \cong \frac{1}{K} G_0(t_0). \tag{25}$$

Attributing $\bar{1}$ to the E_2 state, we will then have $n=n_1=n_{ex}$ and $\bar{n}=n_2$, which qualitatively resembles the intensity dependence shown in Fig. 4(a). Note that, according to Eq. (22), to obtain the linear dependence described by Eq. (25), the excited state absorption of the E_1 state should compensate the ground state bleaching in spectral region of the E_2 transition.

Numerical solution of Eq. (20) provides quantitatively the time evolution of $n_1 \equiv n$ and $n_2 \equiv \bar{n}$, which can be compared with the experimental kinetics. Representative results of such calculations are shown in Fig. 7 by assuming the following parameters: $1/K=20$ fs, $\gamma=2\Gamma=0.8$ ps^{-1}, and a Gaussian generation function $G(t)$ with a pulse duration of 100 fs and an intensity of ten excitons per nanotube. The relaxation rate K determines the ratio of the maximum values of n_1 and n_2, and the chosen K value gives a ratio of ~20 which is similar to the experimental ratio. However, the values of the annihilation rate γ and the integral intensity of the exciton generation are coupled. For instance, a qualitatively similar result can be obtained by increasing the integral intensity of the exciton generation by ten times and, at the same time, decreasing the annihilation rate by the same amount. To obtain absolute values for these two parameters, one must independently determine the population of the E_1 excitons created in a given tube type at different excitation intensities. This determination requires an accurate absorption cross section per tube and the portion of excitons that dissociate into electron-hole pairs.[21] Both the cross section and the yield of exciton dissociation are currently unavailable, and therefore we do not pursue a numerical simulation of the experimental data. Nevertheless, the numerical results shown in Fig. 7 reproduce the experimental relationship between $n_1(t)$ and $n_2(t)$ [see Fig. 4(b)], i.e., $n_2(t) \propto n_1^2(t)$. In addition, the intensity dependence of the maximum populations of n_1 and n_2 can be also obtained by the numerical calculations as shown in Fig. 8, which follow the qualitative dependence predicted by Eqs. (24) and (25). The dependence is also consistent with the experimental results shown in Fig. 4(a).

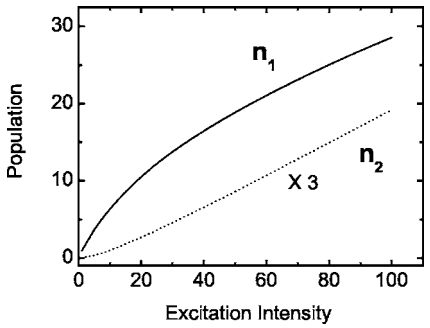

FIG. 8. Plot of the maximum populations of the E_1 (solid line) and E_2 (dashed line) states vs excitation intensity of the E_1 state (in number of excitons per tube) calculated numerically via Eq. (20).

The total exciton population is equal to the sum over all exciton manifolds. Since the probability of populating a given exciton manifold should decay exponentially [see Eq. (10)], the kinetics of exciton annihilation can be also described by a sum of exponential components. For instance, the slowest kinetics should correspond to an exponential term with a linear decay rate k, and the next exponent should decay with a rate $2(k+\Gamma)$. The presence of the annihilation rate Γ in the exponent means that exponential functions can be used to describe the kinetics of exciton-exciton annihilation, and this approach was used previously to analyze the data of quantum dots.[53]

The generation of coherent excitons, necessarily leads to extremely rapid annihilation and prevents the creation and maintenance of high densities of excitation population in semiconducting nanotubes as noted by others.[19] Consequently, those applications replying on a high density of population will require tailoring the inherent electronic properties to generate long-lived excited state(s). Moreover, this rapid annihilation will also produce a substantial amount of excess energy on a very short time scale, which may induce other dynamical processes such as exciton dissociation, cooling of exciton or charged carriers, etc. Identification and characterisation of these processes await future studies.

Exciton-exciton annihilation is also an important component of the excitation kinetics of other nanoscale semiconducting systems, such as quantum rods and wires,[41,42] to which the theoretical description presented in this paper should also be applicable. However, exciton-exciton annihilation in SWNTs appears exceptionally fast, being at least one order of magnitude faster than the corresponding annihilation rates determined for semiconducting quantum rods and wires. This difference can presumably be attributed to very different exciton-phonon coupling and/or distribution of the manifold of states responsible for the annihilation. As follows from Eq. (6), the rate $\Gamma_{2\to\bar{1}}$ is strongly dependent on the density of $\bar{1}$ states, and the maximum rate is obtained

when the reacting excitons and the corresponding product states have small energy gaps. Another difference between quantum rods and wires and SWNT may be in the coherence length of the exciton. If the physical length of the system substantially exceeds the coherence length, exciton-exciton annihilation will become a diffusion-limited process and the annihilation rate will decrease.

The formulas derived for describing the coherent exciton based annihilation process can be used to discuss the excitonic versus uncorrelated electron and hole pairs models of the elementary excitations in semiconducting SWNT. A determination of the nature of the elementary excitations is clearly of central importance for understanding the fundamental physics of these materials.

To see how the two pictures of the elementary excitations can be distinguished, we begin by assuming that the elementary excitations created by absorbing photons are uncorrelated charged carriers, i.e., electrons and holes (e-h). In this case, the dependence of the fluorescence and transient absorption kinetic decays on the excitation intensity [see, for example, Figs. 1(a) and 3(a)] can be attributed to the so-called Auger recombination processes, a nonlinear process involving three charged carriers[45,53,54]

$$\frac{dn_{e,h}}{dt} = -\frac{1}{3}\gamma_A n_{e,h}^3, \tag{26}$$

where $n_{e,h}$ is the population of the charge carriers and γ_A is the rate of the three-particle Auger recombination. The population kinetics determined by Eq. (26) gives the following relationship: $[n_{e,h}(0)/n_{eh}(t)]^2 - 1 = \gamma_A n_{e,h}^2(0)t$, where $n_{e,h}(0)$ is the initial population of charge carriers. Since the fluorescence emission results from electron-hole recombination, its intensity $I(t)$ at a given delay time t is proportional to $n_{e,h}^2(t)$. As a result, the inverse of the fluorescence intensity, $1/I(t)$, will scale linearly with t. Because the same linear dependence is also predicted from the exciton-exciton annihilation [see the solution of Eq. (1)], we conclude that, from time-resolved fluorescence data recorded with high intensity excitation when annihilation dominates the overall relaxation, it is not possible to identify the nature of elementary excitations in semiconducting SWNT as either neutral excitons or charge carriers.

In contrast, exciton-exciton annihilation and the Auger recombination involving three charge carriers predict distinct time dependence for the kinetics recorded with transient absorption spectroscopy. In this case, the amplitude of the bleaching signal [$\Delta\mathrm{OD}(t)$] is always determined by population regardless of the nature of the elementary excitations [see Eq. (22)].[55] According to the solutions of Eqs. (1) and (26), a linear time dependence is found for $1/\Delta\mathrm{OD}(t)$ when exciton-exciton annihilation dominates the kinetics, or for $1/[\Delta\mathrm{OD}(t)]^2$ when Auger recombination of charged carriers dominants the kinetics. As follows from Figs. 3(b) and 3(d), a linear time dependence is observed for $1/\Delta\mathrm{OD}(t)$ but not for $1/[\Delta\mathrm{OD}(t)]^2$, thus suggesting an excitonic nature of the elementary excitations. We note that the same approach has been applied to distinguish the nature of elementary excitations in semiconductor quantum rods, though no justification was given for applying a time-independent annihilation rate to the nonlinear exciton relaxation in this quasi-1D system.[45]

VI. CONCLUDING REMARKS

The theoretical description of nonlinear annihilation involving coherent excitons developed in this paper provides a consistent basis for analysis of the excitation-intensity-dependent decay kinetics measured using femtosecond fluorescence and transient absorption techniques for selected semiconducting nanotube species. In particular the analysis provides a firm basis for the use of a time-independent exciton annihilation rate. Numerical calculations based on our formalism enable us to qualitatively reproduce all the features of the experimental data. For example the relationship between the time evolution of the populations in the two lowest excitonic states and their intensity dependences are well described. The formalism will enable extraction of the linear relaxation from E_2 state to E_1 state and the annihilation rate by quantitative simulations of the experimental data, provided that the number of excitons created per tube under a given excitation intensity can be accurately determined. It is also demonstrated that kinetics arising from exciton-exciton annihilation can be distinguished from the nonlinear Auger recombination of the unbound electrons and holes. Thus, application of the model should enable identification of the nature of the elementary excitations in semiconducting SWNT in a straightforward manner.

As a final remark, it is worth mentioning that the intensity dependence described by Eqs. (24) and (25) is also observed for a semiconducting zigzag tube type, the (11,0) tube. However, the time evolution of the populations in the corresponding E_1 and E_2 states deviates clearly from the results shown in Figs. 4(b), 4(c), and 7. We believe that this deviation arises from a remarkably low population of excitons created due to use of a lower pump intensity, and/or to possibly a smaller absorption cross section of this selected tube type. A detailed account of these results will be reported elsewhere.

ACKNOWLEDGMENTS

This work was supported by the NSF. L.V. thanks the Fulbright Foundation for financial support. We thank J. Stenger and J. Zimmermann for their contributions to the experiments, S. L. Dexheimer for helpful discussion, and S. M. Bachilo and R. E. Smalley for generously providing the HiPco SWNT materials.

*Author to whom correspondence should be addressed. Electronic address: grfleming@lbl.gov

[1] M. S. Dresselhaus, G. Dresselhaus, and P. C. Eklund, *Science of Fullerenes and Carbon Nanotubes* (Academic, San Diego, 1996).

[2] S. Saito, G. Dresselhaus, and M. S. Dresselhaus, *Physical Properties of Carbon Nanotubes* (Imperial College Press, London, 1998).

[3] R. H. Baughman, A. A. Zakhidov, and W. A. de Heer, Science **297**, 787 (2002).
[4] A. J. Heeger, in *Primary Photoexcitations in Conjugated Polymers: Molecular Excitation Versus Semiconductor Band Model*, edited by N. S. Sariciftci (World Scientific, Singapore, 1997), p. 20.
[5] A. Hagen, G. Moos, V. Talalaev, and T. Hertel, Appl. Phys. A **78**, 1137 (2004).
[6] T. W. Odom, J.-L. Huang, P. Kim, and C. M. Lieber, J. Phys. Chem. B **104**, 2794 (2000).
[7] G. N. Ostojic, S. Zaric, J. Kono, M. S. Strano, V. C. Moore, R. H. Hauge, and R. E. Smalley, Phys. Rev. Lett. **92**, 117402 (2004).
[8] C. D. Spataru, S. Ismail-Beigi, L. X. Benedict, and S. G. Louie, Appl. Phys. A **78**, 1129 (2004).
[9] C. D. Spataru, S. Ismail-Beigi, L. X. Benedict, and S. G. Louie, Phys. Rev. Lett. **92**, 077402 (2004).
[10] J.-S. Lauret, C. Voisin, G. Cassabois, C. Delalande, P. Roussignol, O. Jost, and L. Capes, Phys. Rev. Lett. **90**, 057404 (2003).
[11] O. J. Korovyanko, C.-X. Sheng, Z. V. Vardeny, A. B. Dalton, and R. H. Baughman, Phys. Rev. Lett. **92**, 017403 (2004).
[12] L. Huang, H. N. Pedrosa, and T. D. Krauss, Phys. Rev. Lett. **93**, 017403 (2004).
[13] Y.-Z. Ma, L. Valkunas, S. L. Dexheimer, S. M. Bachilo, and G. R. Fleming, Phys. Rev. Lett. **94**, 157402 (2005).
[14] I. V. Rubtsov, R. M. Russo, T. Albers, P. Deria, D. E. Luzzi, and M. J. Therien, Appl. Phys. A **79**, 1747 (2004).
[15] H. Hippler, A.-N. Unterreiner, J.-P. Yang, S. Lebedkin, and M. M. Kappes, Phys. Chem. Chem. Phys. **6**, 2387 (2004).
[16] J.-P. Yang, M. M. Kappes, H. Hippler, and A.-N. Unterreiner, Phys. Chem. Chem. Phys. **7**, 512 (2005).
[17] Y.-Z. Ma, J. Stenger, J. Zimmermann, S. M. Bachilo, R. E. Smalley, R. B. Weisman, and G. R. Fleming, J. Chem. Phys. **120**, 3368 (2004).
[18] F. Wang, G. Dukovic, L. E. Brus, and T. F. Heinz, Phys. Rev. Lett. **92**, 177401 (2004).
[19] F. Wang, G. Dukovic, E. Knoesel, L. E. Brus, and T. F. Heinz, Phys. Rev. B **70**, 241403(R) (2004).
[20] Y.-Z. Ma, L. Valkunas, S. L. Dexheimer, and G. R. Fleming, Mol. Phys. (to be published).
[21] Y.-Z. Ma, L. Valkunas, S. M. Bachilo, and G. R. Fleming, J. Phys. Chem. B **109**, 15671 (2005).
[22] F. Wang, G. Dukovic, L. E. Brus, and T. F. Heinz, Science **308**, 838 (2005).
[23] J. Maultzsch, R. Pomraenke, S. Reich, E. Chang, D. Prezzi, A. Ruini, E. Molinari, M. S. Strano, C. Thomsen, and C. Lienau, Phys. Rev. B **72**, 241402(R) (2005).
[24] V. M. Agranovich and M. D. Galanin, *Electronic Excitation Energy Transfer in Condensed Matter* (North-Holland, Amsterdam, 1982).
[25] M. Pope and C. E. Swenberg, *Electronic Processes in Organic Crystals* (Oxford University Press, New York, 1999).
[26] L. Valkunas, G. Trinkunas, and V. Liuolia, in *Resonance Energy Transfer*, edited by D. L. Andrews and A. A. Demidov (Wiley, Chichester, 1999), p. 244.
[27] H. van Amerongen, L. Valkunas, and R. van Grondelle, *Photosynthetic Excitons* (World Scientific, Singapore, 2000).
[28] A. A. Ovchinikov, S. F. Timashev, and A. A. Belyi, *Kinetics of Diffusion-Controlled Chemical Processes* (Nova, New York, 1989).
[29] A. Suna, Phys. Rev. B **1**, 1716 (1970).
[30] D. Mauzerall, Biophys. J. **16**, 87 (1976).
[31] G. Paillotin, C. E. Swenberg, J. Breton, and N. E. Geacintov, Biophys. J. **25**, 513 (1979).
[32] E. Kotomin and V. Kuzovkov, Rep. Prog. Phys. **51**, 1479 (1988).
[33] E. Kotomin and V. Kuzovkov, Rep. Prog. Phys. **55**, 2079 (1992).
[34] R. F. Khairutdinov and N. Serpone, Prog. React. Kinet. **21**, 1 (1996).
[35] W. T. F. den Hollander, J. G. C. Bakker, and R. van Grondelle, Biochim. Biophys. Acta **725**, 492 (1983).
[36] R. van Grondelle, Biochim. Biophys. Acta **811**, 147 (1985).
[37] L. Valkunas, G. Trinkunas, V. Liuolia, and R. van Grondelle, Biophys. J. **69**, 1117 (1995).
[38] G. Trinkunas, J. L. Herek, T. Polivka, V. Sundström, and T. Pullerits, Phys. Rev. Lett. **86**, 4167 (2001).
[39] S. Havlin and A. Bunde, in *Fractals and Disordered Systems*, edited by A. Bunde and S. Havlin (Springer-Verlag, Berlin, 1991), p. 97.
[40] L. Valkunas, E. Akesson, T. Pullerits, and V. Sundström, Biophys. J. **70**, 2373 (1996).
[41] B. Bruggemann and V. May, J. Chem. Phys. **118**, 746 (2003).
[42] B. Bruggemann and V. May, J. Chem. Phys. **120**, 2325 (2004).
[43] A. V. Barzykin and M. Tachiya, Phys. Rev. B **72**, 075425 (2005).
[44] M. J. O'Connell, S. M. Bachilo, C. B. Huffman, V. C. Moore, M. S. Strano, E. H. Haroz, K. L. Rialon, P. J. Boul, W. H. Noon, C. Kittrell, J. Ma, R. H. Hauge, R. B. Weisman, and R. E. Smalley, Science **297**, 593 (2002).
[45] H. Htoon, J. A. Hollingsworth, R. Dickerson, and V. I. Klimov, Phys. Rev. Lett. **91**, 227401 (2003).
[46] H. Zhao and S. Mazumdar, Phys. Rev. Lett. **93**, 157402 (2004).
[47] C. D. Spataru, S. Ismail-Beigi, R. B. Capaz, and S. G. Louie, Phys. Rev. Lett. **95**, 247402 (2005).
[48] Y.-Z. Ma, C. D. Spataru, L. Valkunas, S. G. Louie, and G. R. Fleming (unpublished).
[49] R. Loudon, Am. J. Phys. **27**, 649 (1959).
[50] M. Damnjanovic, I. Milosevic, T. Vukovic, and R. Sredanovic, Phys. Rev. B **60**, 2728 (1999).
[51] N. G. van Kampen, *Stochastic Processes in Physics and Chemistry* (North-Holland, Amsterdam, 1992).
[52] C. Manzoni, A. Gambetta, E. Menna, M. Meneghetti, G. Lanzani, and G. Cerullo, Phys. Rev. Lett. **94**, 207401 (2005).
[53] V. I. Klimov, A. A. Mikhailovsky, D. W. McBranch, C. A. Leatherdale, and M. G. Bawendi, Science **287**, 1011 (2000).
[54] M. Ghanassi, M. C. Schanne-Klein, F. Hache, A. I. Ekimov, D. Ricard, and C. Flytzanis, Appl. Phys. Lett. **62**, 78 (1993).
[55] J. Shah, *Ultrafast Spectroscopy of Semiconductors and Semiconductor Nanostructures* (Springer-Verlag, Berlin, 1999).